

NMR Characterization of the Formation Kinetics and Structure of Di-O-Benzylidene Sorbitol Gels Self-Assembled in Organic Solvents

David L. VanderHart,* Jack F. Douglas,* Steven D. Hudson, Joseph M. Antonucci, and Elizabeth A. Wilder†

Polymers Division, National Institute of Standards and Technology, Gaithersburg, Maryland 20899, United States. †Present address: Procter and Gamble, Cincinnati, Ohio 45252, United States

Received March 30, 2010. Revised Manuscript Received December 8, 2010

The molecule 1,3:2,4-di-*O*-benzylidene sorbitol (DBS) is a common “gelator” that forms thermally reversible gels in diverse organic solvents. Solid-state ^{13}C and ^1H NMR techniques, along with electron microscopy, are utilized in an exploratory study of DBS in the gelled state where we consider both in situ and dried gels. The gels were formed in either acetone or benzene, with the former being a better solvent for DBS. We find the in situ or dried DBS gels to be composed of rigid twisted nanofibrils (~ 15 to 21 nm in diameter). The fibrils show local molecular ordering, but not crystalline order, and they contain no trapped solvent. The molecular mobility at the fibril surface is modestly enhanced, and all the free hydroxyl groups of the sorbitol moiety are involved in strong hydrogen bonding. We also attempted to find a truly crystalline form of DBS whose structure, as judged by the similarity of ^{13}C spectra, is close to that of the fibrils. We partially succeeded in this quest, employing melt crystallization followed by slow cooling. However, this sample was a mixed crystal having small domains, where only one type of domain was structurally similar to the fibrils. We also investigated the long-time evolution of the in situ DBS gel network. Specifically, high-resolution NMR kinetic studies were performed over periods of days where the residual concentration of DBS in acetone solution was monitored during and after gel formation. The DBS concentration on these long timescales evolved slowly, and we introduce a simple mathematical model and equation to describe this phenomenon.

Introduction

Chiral molecule 1,3:2,4-di-*O*-benzylidene sorbitol (DBS) is known to form thermally reversible gels in many organic solvents,^{1–4} even at concentrations in the range of 0.5 to 1% DBS volume fraction. Its propensity for gel formation also makes it attractive as a nucleating agent for synthetic polymers such as isotactic polypropylene.⁵ DBS has also found applications in cosmetic formulations.^{2,3} The gels that form from these materials are often optically clear, indicating in the general case where there is scattering contrast between the DBS and the surrounding medium that the solid-state dimensions (including the cross-sectional dimensions of the DBS gel fibers within these structures) are well below the wavelengths of visible light. In fact, DBS gel fiber cross-sectional dimensions of as small as 3.2 nm have been reported⁶ for some isolated and dried DBS fibrils, but the fiber diameters are more typically found in the 10 to 80 nm range⁷ where solvent polarity is often noted as a relevant factor in this wide variation.⁴ It has also been suggested that some of the larger-diameter fibrils are aggregates of smaller fibrils whose diameters are about 10 nm.⁷ A competition of H-bonding interactions involving DBS with the solvent or DBS with itself is often discussed in connection

with fibril formation,⁴ but the details remain poorly understood from a quantitative standpoint.

It is generally presumed that fiber formation (and subsequent gel formation from networks of these fibers) produces long-range, but not necessarily crystalline, solid-state order. In DBS, molecular ordering is believed to arise from a local stacking of molecules, where directional hydrogen bonding between sorbitol functional groups (hydroxyl groups, ether oxygens) and possibly π – π bonding between stacked aromatic rings of the benzylidene units are deemed important for this self-assembly process.⁸ The fibers can be considered to be a bundle of these molecular stacks or “threads”. The fact that gelation fails when the C6 hydroxyl of DBS becomes a methoxyl group, while gelation is still possible when the C5 hydroxyl is similarly modified,⁶ has been interpreted to signify that the C6 hydroxyl forms a crucial hydrogen bond required for fiber formation. It is also clear that the lateral dimensions of the gel fibrils are all well above the dimensions of the individual molecule. As mentioned before, an intriguing aspect of this type of gelation process is the emergence of fibers having well-defined widths, which vary somewhat with the thermodynamic conditions, including the type of solvent.

A characteristic feature of DBS fibril formation is the slow helical twisting of the fibers.^{4,7,9} One would like to understand whether the chirality of DBS is responsible for this effect or whether the phenomenon is more general. The combined behaviors of helically twisted fiber formation and thermally reversible gelation seen in DBS also occur with other gelators¹⁰ as well as diverse proteins. Hence, an understanding of the origin of such structures is a matter of wide interest. In particular, protein fiber and gel

*Corresponding authors. E-mail: david.vanderhart@nist.gov, jack.douglas@nist.gov.

(1) Wolfe, J. K.; Hann, R. M.; Hudson, C. S. *J. Am. Chem. Soc.* **1942**, *64*, 1493. Yamamoto, S. *Kogyo Kagaku Zasshi* **1942**, *45*, 695.

(2) Roehl, E.-L.; Tan, H.-B. U.S. Patent 4,154,816, May 15, 1979. Randhawa, M. H.; Schamper, T. J. U.S. Patent 4,719,102, Jan 12, 1988.

(3) Lin, Y. C.; Kachar, B.; Weiss, R. G. *J. Am. Chem. Soc.* **1989**, *111*, 5542.

(4) Yamasaki, S.; Tsutsumi, H. *Bull. Chem. Soc. Jpn.* **1995**, *68*, 123.

(5) DiNardo, V. M. U.S. Patent 4,514,534, Apr 30, 1985.

(6) Yamasaki, S.; Ohashi, Y.; Tsutsumi, H.; Tsujii, K. *Bull. Chem. Soc. Jpn.* **1995**, *68*, 146.

(7) Wilder, E. A.; Hall, C. K.; Khan, S. A.; Spontak, R. J. *Langmuir* **2003**, *19*, 6004.

(8) Wilder, E. A.; Spontak, R. J.; Hall, C. K. *Mol. Phys.* **2003**, *101*, 3017.

(9) Thierry, A.; Fillon, B.; Straupe, C.; Lotz, B.; Wittmann, J. C. *Prog. Colloid Polym. Sci.* **1992**, *87*, 28.

(10) Terech, P.; Weiss, R. G. *Chem. Rev.* **1997**, *97*, 3133.

formation are associated with many serious diseases such as Alzheimer's, Huntington's, Parkinson's, and sickle cell disease, type II diabetes, mad cow disease, scrapie, and other prion diseases.^{11–14} A greater understanding of this type of growth process thus has the potential for significant application to both biology and materials science.

Both limited lateral growth and helical twisting on supramolecular distance scales greatly lower any expectation of well-defined crystallinity because none of the accepted types of crystalline unit cells, from geometrical considerations only, form crystalline structures with either limited lateral growth or with twisting architecture. Helicity, by definition, incorporates some aspect of circular geometry, whereas traditional unit cells assemble only along linear loci. (It is important to note that molecular helicity within a unit cell is completely acceptable; however, this results in side-by-side, independent helices.) Nevertheless, it is certainly conceivable that some molecular system may want to condense into an elementary structure (e.g., a sheet) that possesses some curvature. The general point is that one cannot stack surfaces having curvature without distorting that curvature if one insists that the surfaces can seek their van der Waals' energy minima along the entire contour. That is to say, one can always stack very rigid curved entities (e.g., curved sheets of uniform thickness). Nevertheless, it is geometrically impossible to stack such sheets, curve on top of curve, without producing forces that would lead to geometric distortion because sheet-to-sheet separation, measured along the direction of the local surface normal, is not maintained over the entire contour. Therefore, in this article, we restrict our definition of "true" crystallization to those structures whose unit cells are invariant throughout the crystalline domain.

When a material such as DBS is seen to have a helically fibrillar morphology (i.e., ordered but not fully crystalline and limited in lateral growth), the foregoing ideas may come into play in explaining this morphology. In particular, two notions are invoked. First, the fibrils may possess some elementary structure where there is curvature in some plane normal to the fibril axis. Second, lateral growth of the fibril probably involves the stacking of these elementary structures so that growth most likely takes place with increasing distortion in the outer layers. Then the final diameter of the fibril cannot exceed that diameter where the free-energy costs of the distortion offset the free-energy gains from deposition. A couple of examples in the literature where such interplays have been invoked are (a) Turner et al.,¹⁵ who describe how the fibril diameter and helical pitch are inversely related in sickled hemoglobin (a lower helical pitch means a slower buildup of distortion energy with fibril diameter) and (b) a very detailed study^{16,17} of an 11-peptide protein that forms a curved, β -sheet elementary structure that further self-assembles into larger aggregates, including fibrils of limited lateral size, whose dimensions are interpreted in terms of distortion energies that accompany the aggregation of the elementary structures.

Other basic ideas for producing helical fibers of limited lateral dimension exist. For example, Fejer et al.¹⁸ and Huisman et al.¹⁹ have recently shown that helical fiber geometries can arise from a direct competition between molecular interactions (molecular shape and van der Waals interactions in their particular calculations) that create a minimum in the potential of the interacting particles along a direction normal to fiber growth. Such secondary interaction minima naturally exist in dipolar fluids²⁰ (gelators and proteins often have large dipole moments^{21,22}), so this idea also seems to have merit.²³

We also point out that protein fibers have commonly been observed to form superfibrils composed of "protofilament" fibrils, and these superfibrils may in turn organize into higher-order twisted fiber structures so that hierarchical fiber structures form.

We used transmission electron microscopy (TEM) to monitor the diameter of certain dried DBS fibrils that were obtained from DBS gels in two solvents, acetone and benzene. Additionally, we measured the kinetics of DBS gelation in acetone in order to examine the slow evolution of the gel structure at long times by NMR and to check the consistency of the observed DBS gel assembly kinetics with the conceptual models described above. Because we also used a solid-state proton probe to investigate in situ DBS gels in deuterated solvents, we were then in a position to observe the proton spectrum of the gelled structure so as to compare it with the proton spectrum of the pure DBS solid. This allowed us to determine whether the solvent was trapped in the DBS gel fiber structure.

This work is an exploration of DBS gelation and properties rather than a systematic investigation of DBS gelation.

Experimental Section

Materials. A powder sample of DBS was obtained from Milliken (lot no. R1121) and was used without further purification. (Certain equipment, instruments, or materials are identified in this article in order to specify the experimental details adequately. Such identification does not imply a recommendation by the National Institute of Standards and Technology nor does it imply that the materials are necessarily the best available for the purpose.) We denote this material "as received". In those cases where deuterated solvents were used, the isotopic enrichment was 99.9%.

Sample Preparation. Acetone and benzene were chosen as the two main solvents to be investigated for the in situ DBS gels. Two types of gel samples were made: one for high-resolution observation of the DBS remaining in solution and the other for the observation of solid-state NMR spectra of DBS in the gels.

For the high-resolution NMR measurements, we loaded DBS and solvent directly into NMR tubes, freezing the contents in liquid nitrogen on a vacuum line, pumping out the gases, reintroducing either air or nitrogen at a pressure slightly below atmospheric, and then sealing the tubes. Sample dissolution was initiated at various temperatures, always at least 110 °C, by preheating a 2.5-cm-o.d. copper rod having an 18-cm-deep 5.3-mm-i.d. hole, putting the copper rod in a thermal sleeve, introducing the entire length of the NMR tube into the hole in the rod, and allowing for dissolution for about 3 min with constant inversion and mixing

(11) Khurana, R.; Ionescu-Zanetti, C.; Pope, M.; Li, J.; Nielson, L.; Ramirez-Alvarado, M.; Regan, L.; Fink, A. L.; Carter, C. A. *Biophys. J.* **2003**, *85*, 1135.

(12) Manno, M.; Craparo, E.; Martorana, V.; Bulone, D.; San Biagio, P. *Biophys. J.* **2006**, *90*, 4585.

(13) Librizzi, F.; Rischel, C. *Protein Sci.* **2005**, *14*, 3129.

(14) Hamilton-Brown, P.; Bekard, I.; Ducker, W. A.; Dunstan, D. E. *J. Phys. Chem. B* **2008**, *112*, 16249.

(15) Turner, M. S.; Briehl, R. W.; Ferrone, F. A.; Josephs, R. *Phys. Rev. Lett.* **2003**, *90*, 128103.

(16) Nyrkova, I. A.; Semenov, A. N.; Aggeli, A.; Boden, N. *Eur. Phys. J.* **2000**, *17*, 481.

(17) Nyrkova, I. A.; Semenov, A. N.; Aggeli, A.; Bell, M.; Boden, N.; MacLeish, T. C. B. *Eur. Phys. J.* **2000**, *17*, 499.

(18) Fejer, S. N.; Wales, D. J. *Phys. Rev. Lett.* **2007**, *99*, 086106.

(19) Huisman, B. A. H.; Bolhuis, P. G.; Fasolino, A. *Phys. Rev. Lett.* **2008**, *100*, 188301.

(20) Van Workum, K.; Douglas, J. F. *Phys. Rev. E* **2005**, *71*, 031502.

(21) Brotin, T.; Utermohlen, R.; Fages, F.; Bouas-Laurent, H.; Desvergne, J. P. *J. Chem. Soc., Chem. Commun.* **1991**, 416.

(22) Sakamoto, A.; Ogata, D.; Shikata, T.; Urakawa, O.; Hanabusa, K. *Polymer* **2006**, *47*, 956.

(23) Chakrabarti, D.; Fejer, S. N.; Wales, D. J. *Proc. Natl. Acad. Sci. U.S.A.* **2009**, *106*, 20164.

in the tube. These samples were then taken from the tube and cooled (rather rapidly) in air. This method of heating was adopted because it allowed constant mixing, gave uniform and efficient heating so as to minimize any chemical degradation that might take place, and could safely contain any explosion of the tube (we went up as high as 140 °C, where the vapor pressures of the solvents were well above atmospheric pressure).

The other type of sample was intended for solid-state studies using a solid-state proton probe. There, the primary consideration was the maintenance of the entire sample well within the rf coil so that excitation of the solid phase in the DBS could be optimized. Pyrex 5 mm tube stubs were used. Small, weighed submilligram DBS samples were introduced into the tube. The tube was then "necked" with a torch about 2.2 cm from the bottom, weighed, and placed on a vacuum line. After evacuation, approximately 4 mm of solvent was introduced into each tube by distillation. Samples were then sealed under a nitrogen pressure that was slightly below ambient pressure. Samples, in total length, were less than 2.5 cm. Finally, the amount of solvent distilled was determined gravimetrically. For initiation, all of the latter samples were heated in an oven to 100 °C, where dissolution was complete, and then were cooled slowly in the turned-off oven and left at ambient temperature (22 °C).

Besides the foregoing in situ gel samples, solid forms of DBS were also prepared in order to understand the solid-state organization of the gel-phase DBS better. To this end, 200 mg quantities of DBS were prepared from a 2.3% DBS-in-acetone gel and from a 2.0% DBS-in-benzene gel. The ingredients were placed in 9-mm-o.d. pyrex tubes, which were then sealed and placed in the oven at 140 °C for the benzene gel and 120 °C for the acetone gel. After being thoroughly mixed, at temperature, the solutions were allowed to cool slowly in the turned-off oven. Cooled tubes were allowed to gel for a day at ambient temperature and then were broken open to allow the solvent to evaporate. The benzene gel–solid should relate especially well to the in situ structure of the gel because, as will be seen, after this period of gelation, less than 3% of the DBS remains in solution, implying that any reorganization of the solids during solvent removal should be minimal.

Last, six solid-state samples were prepared on the basis of melt crystallization. Sealed, evacuated powder samples of DBS were placed in 9 mm pyrex tubes and were inserted into the thermocouple well of a viscometer that was preheated to exactly 230 °C. After about 7 min, the DBS melted completely. One sample, after melting, was cooled slowly in the turned-off viscometer. The initial cooling rate was about 3 °C/min, and this sample was designated MC-SC. Melts of the remaining five samples were immediately removed from the viscometer and allowed to cool in air (sample MC-AC). Three of those samples, MC-AC-100, MC-AC-150, and MC-AC-170, were subsequently annealed at 100, 150, or 170 °C for 18 h and then cooled slowly in the turned-off viscometer. The annealing cycle for the final sample involved sequentially heating to 200 °C, holding there for 5 min, and then decreasing the temperature in 5 °C increments (for 5 min) until reaching 175 °C. The latter temperature was then held for 18 h (sample MC-AC-ramp175). The various annealing cycles were used to investigate and attempt to optimize the solid–solid crystal transformation of the MC-AC samples.

TEM. TEM images of four selected DBS samples were obtained using a Philips EM400T operated at 120 kV in bright-field mode. All samples were dispersed in benzene before deposition onto a mica substrate. Pt was then evaporated at an angle of approximately 26° to produce a shadow whose length is twice that of the object height. The samples were also backed with a layer of carbon before being mounted on a copper grid.

NMR. Proton NMR data were obtained on a Bruker Avance spectrometer (Bruker Biospin Inc. Billerica, MA) operating at 7.05 T (300 MHz for ¹H). Solid-state proton spectra were obtained using a low-background probe made by Doty Scientific (Columbia, SC). This high-power, 5 mm sample probe includes

the capability for magic angle spinning²⁴ (MAS). Typical rf field strengths corresponded to nutation frequencies of 167 kHz. MAS frequencies were typically 2.5 kHz unless a static sample was called for.

Proton experiments employed in this work include (a) the normal Bloch-decay spectra (Fourier transform of the response to a single pulse), (b) saturation–recovery and inversion–recovery experiments²⁵ for determining the longitudinal proton relaxation time, T_1^H , (c) the Carr–Purcell–Meiboom–Gill (CPMG) sequence²⁶ for measuring the transverse proton relaxation time, T_2^H , and (d) the MREV-8 multiple pulse sequence.^{27,28} The latter sequence, when combined with MAS, gives so-called "CRAMPS" spectra (combined rotation and multiple-pulse spectroscopy²⁹), which in turn mainly yield isotropic chemical shift profiles for the protons. Alternatively, by using nonspinning samples and a different prepulse, we can utilize the same basic MREV-8 sequence to monitor a toggling frame relaxation time,³⁰ T_{1xz} , which gives insight into the spectral density of molecular motions, primarily those in the midkilohertz regime. Finally, for cases where we recognized some significant heterogeneity of molecular mobility, we also incorporated the concept of spin diffusion³¹ into the design of our pulse sequences. For spin systems characterized by an extended network of homonuclear-dipolar-coupled spins (protons of most organic solids qualify), spin diffusion is the diffusive movement of polarization, observable in the presence of polarization gradients. Hence, for example, by generating gradients based on differences in molecular mobility (e.g., via T_{1xz} relaxation), one can monitor the rate of the subsequent disappearance of such gradients and thereby obtain information about the spatial separation of the regions associated with the mobility differences. We used two variants of a multiperiod pulse sequence, each based on differential T_{1xz} behavior. The experiments consisted of applying, in the first period, the usual T_{1xz} sequence for an initial, relatively short time where the more-mobile sites decay preferentially compared with the less-mobile sites. One then quickly stores the magnetization as the Zeeman polarization; this marks the beginning of the second, variable, rf-free period (i.e., the spin diffusion (SD) time, t_{sd}). Following this, one monitors the magnetization either by taking another T_{1xz} decay or by taking a Bloch decay, depending on which observable is more insightful for monitoring polarization changes during the spin diffusion time. Respectively, these latter variant experiments are referred to as T_{1xz} - T_{1xz} -SD or T_{1xz} -BD -SD experiments, and both sequences include an inversion of the initial magnetization on alternate scans upon adding and subtracting alternate signals. In this way, T_1^H 's effects on the spin diffusion behavior are reduced and also are more easily separated from the spin diffusion effects. More experimental details regarding these experiments can be found in the Supporting Information.

Cross-polarization and MAS (CPMAS) ¹³C spectra³² were obtained using a noncommercial spectrometer operating at 2.35 T (25 MHz for ¹³C nuclei). Magic-angle spinning at 4 kHz, cross-polarization times of 1 ms, and rf field strengths giving nutation frequencies of 65 and 69 kHz for protons and ¹³C nuclei, respectively, were typical experimental conditions. Experiments include the normal CPMAS experiment³¹ and the measurement of longitudinal ¹³C relaxation times, T_1^C , (method of Torchia³³).

(24) Andrew, E. R. *Prog. Nucl. Magn. Reson. Spectrosc.* **1972**, *8*, 1.

(25) Farrar, T. C.; Becker, E. D. *Pulse and Fourier Transform NMR*; Academic Press: New York, 1971; pp 20–21.

(26) Meiboom, S.; Gill, D. *Rev. Sci. Instrum.* **1958**, *29*, 688.

(27) Rhim, W.-K.; Elleman, D. D.; Vaughan, R. W. *J. Chem. Phys.* **1973**, *59*, 3740.

(28) Mansfield, P.; Orchard, J.; Stalker, D. C.; Richards, K. H. B. *Phys. Rev.* **1973**, *B7*, 90.

(29) Ryan, L. M.; Taylor, R. E.; Paff, A. J.; Gerstein, B. C. *J. Chem. Phys.* **1980**, *72*, 508.

(30) Vega, A. J.; Vaughan, R. W. *J. Chem. Phys.* **1978**, *68*, 1958.

(31) Abragam, A. *The Principles of Nuclear Magnetism*; Oxford University Press: London, 1961; Chapter 5.

(32) Schaefer, J.; Stejskal, E. O.; Buchdahl, R. *Macromolecules* **1975**, *8*, 291.

(33) Torchia, D. A. *J. Magn. Reson.* **1978**, *30*, 613.

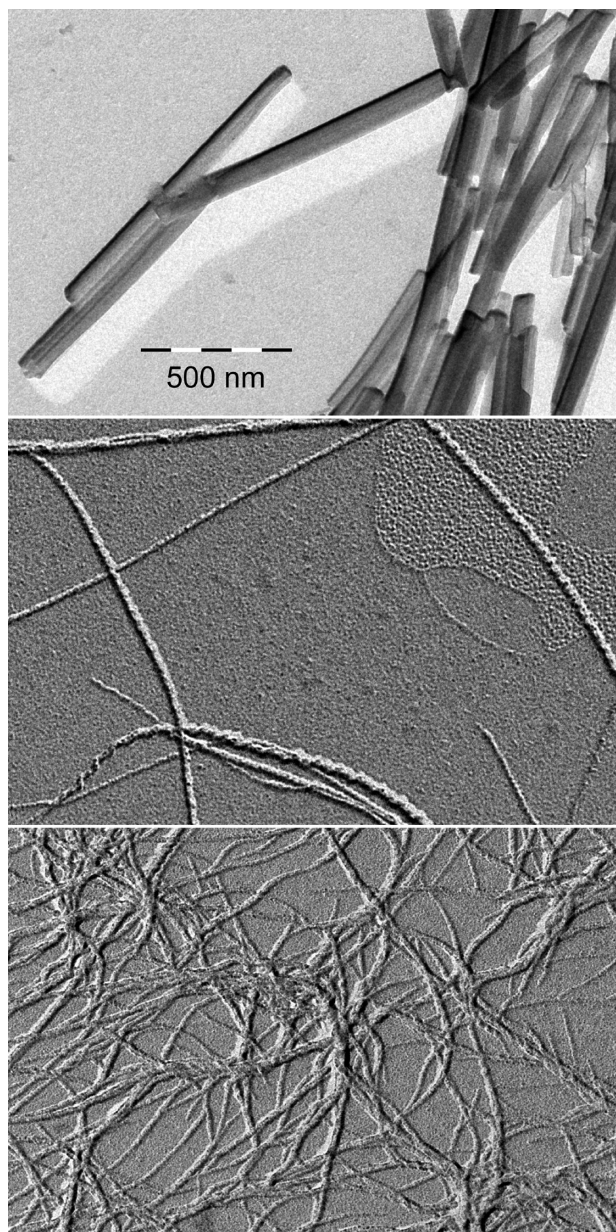
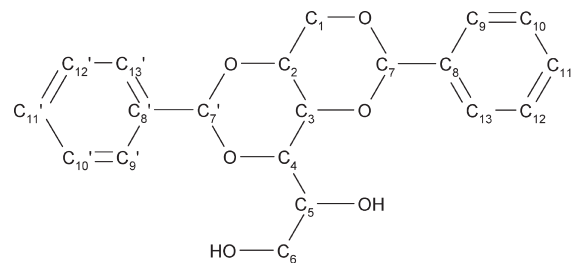


Figure 1. TEM images, each on the same given scale, for different DBS samples. Upper, as received; middle, dried 2.3% DBS in acetone; bottom, dried 2% DBS-in-benzene. Note the indications of helical fibrils. Pt shadowing is such that shadows are twice the width of the object's height.

Additionally, longitudinal and rotating-frame proton relaxation times, T_1^H and $T_{1\rho}^H$, respectively, were measured by varying the recycling delay or the proton spin-locking time prior to cross polarization.

Results

TEM. Four samples were investigated; these included the as-received material as well as three samples of the dried gels (2% DBS-in-benzene, air dried and dried in vacuum for 14 h at 120 °C; and 2.3% DBS in acetone, air dried). Figure 1 shows images of all of the samples except the vacuum-dried sample. TEM images of the latter were not significantly different from those of the air-dried sample. The main features that distinguish the as-received sample from the other two dried-gel samples are that the as-received sample is made up of relatively straight, unbranched



1,3:2,4 Di-O-Benzylidene Sorbitol

Figure 2. Chemical structure of DBS.

rods, about 50 to 60 nm in diameter and $1.5 \pm 0.5 \mu\text{m}$ in length, having no identifiable axial periodicity. In contrast, dried gel fibrils from the acetone and benzene gels are typically not very straight. Dispersion seems incomplete (i.e., there are significant regions where it appears that groups of fibrils have agglomerated). The smaller elements of the dried gel samples are strongly curved and exhibit diameters in the 15 to 30 nm range for the 2.3% DBS-in-acetone sample and in the 15 to 21 nm range for the 2% DBS-in-benzene sample. Branching seems rather frequent in these images; however, it is less clear whether there was branching in the original gel or whether the branching is just the result of individual fibrils peeling away from the agglomerated “trunk” of loosely associated fibrils. Importantly, both of the gel fibrils show evidence of periodicity along the fibril axis. This periodicity is $45 \pm 3 \text{ nm}$ in both samples, which strongly suggests a well-defined fibril helicity. Judging by the uniformly wide shadows for the single fibrils, the cross section of the fibrils is deemed approximately circular, suggesting either that any helical groove on the fibril is shallow or that such periodicity possibly arises from differences in affinity for Pt along the helical fibril. It is also apparent in these images that fibrils twist around other fibrils, leading to fibers with a hierarchal structure.

No TEM images were taken for the melt-crystallized samples because our focus was the gel state. We did observe, however, that both the air-cooled and slowly cooled samples displayed weak cleavage planes and needlelike fragments under an optical microscope. Thus, these samples also showed evidence of a highly preferred growth direction.

^{13}C CPMAS Spectra of Various DBS Solids. ^{13}C spectra (25 MHz) of dried solids were used to monitor, qualitatively, the relative local order in the gel–solids as well as in other, more ordered states of crystallinity. Figure 2 shows the chemical structure of DBS, and Figure 3 gives the ^{13}C spectra, identified in the caption, of several preparations of DBS solids. Of note are spectral differences, indicating either chemical or structural instability, that arise from a 15 day aging period for the melt-crystallized, air-cooled (MC-AC) sample in Figure 3E,F. The primary reason for investigating the melt-crystallized samples was to identify some readily prepared crystalline state that would relate, by virtue of spectral similarity, to the state of order in the gel–solids. All spectra of gel–solids were the same, within experimental uncertainty. Hence, the spectra in Figure 3A,B are representative of all of the gel–solids we examined. Melt-crystallized samples show the sharpest spectral features, which implies more perfect crystalline order, the greatest molecular rigidity, the largest crystallite size, or some combination thereof.³⁴

^{13}C Spectral Assignment. Chemical shifts and relative intensities provide input into assignments. Our working assignment

(34) VanderHart, D. L.; Earl, W. L.; Garroway, A. N. *J. Magn. Reson.* **1981**, *44*, 361.

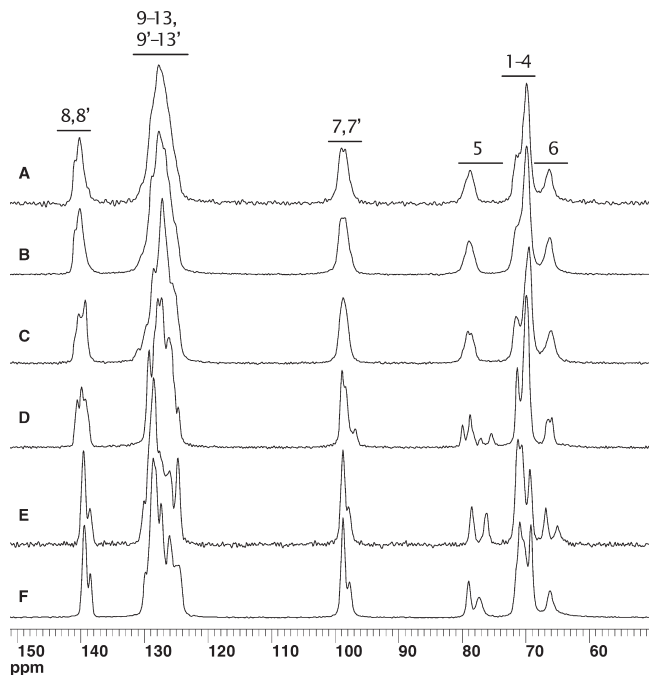


Figure 3. ^{13}C spectra (25 MHz) of various dry DBS preparations. (A) Dried gel from 2% DBS-in-benzene, (B) dried gel from 2.3% DBS in acetone, (C) as received, (D) melt crystallized and slowly cooled (MC-SC), (E) MC and air cooled (MC-AC, fresh), and (F) MC-AC after 15 days of aging with some exposure to humidity. The resonance assignments shown refer to labels in Figure 2.

of shifts to the various carbons, or groups of carbons, in the given DBS structure is also indicated in Figure 3. For the purposes of this article, we are most interested in the proper assignment of the hydroxymethylene carbon (C6) and the hydroxymethine carbon (C5) because these have the most conformational flexibility and the most opportunity to experience variable hydrogen-bonding interactions. Corresponding line shapes and relaxation behaviors might then be most indicative of how the hydrogen-bonding strength changes with the various structures. Unambiguous assignments to individual or groups of carbons include all of those above 84 ppm. One has to be more careful about individual assignments in the region from 65 to 82 ppm because in the solid state resonances can be influenced by conformation³⁵ and probably³⁶ by hydrogen-bonding interactions as well. The assignments for C5 and C6, indicated in Figure 3, are supported by the following evidence: (1) Spectral editing using the polarization/depolarization method³⁷ shows (Supporting Information) that the indicated C5 and C6 regions correspond to a methine and methylene carbon, respectively. (2) These regions are also those that show the largest variability in chemical shift, consistent with expectations from conformation and hydrogen-bonding considerations. (3) Relative integrals confirm the assignment to one carbon for each region. (4) Site-specific dynamics, inferred via relaxation measurements to be discussed, verify that C6 and C5 typically show more mobility than other sites when mobility differences are present. (5) It is typical³⁴ that pendant hydroxymethylene carbons resonate at the highest field in carbohydrates of broadly related structures.

DBS Crystal State with Spectral Similarity to the Gel-Solids. The lack of spectral resolution in Figure 3A,B relative to

that in Figure 3D–F suggests that the DBS fibrils lack the high degree of order associated with a crystalline state. We thought it would be useful, nevertheless, to seek some crystalline state, which could be readily prepared, whose array of chemical shifts closely paralleled that of the gel–solid spectra. If we could find such a crystalline state, then there would be a better chance that an X-ray structure of the melt-crystallized material could be obtained with the result that the approximate structure of the DBS fibril could be inferred.

On the basis of the spectra of Figure 3, the as-received sample has a spectrum (Figure 3C) with similar chemical shifts and slightly better resolution compared with that of the gel–solids (Figure 3A,B). However, the resolution in Figure 3C is not adequate to claim good crystallinity; moreover, the preparation of the as-received sample is proprietary, and we did not have access to the recipe for preparing this material. The spectra (Figure 3E,F) of the MC-AC sample, while featuring better resolution, depart significantly from that of the gel–solids. Notable differences occur in the overall shapes for the two aromatic regions (124–142 ppm) as well as for the 68–73 ppm band. Therefore, we dismiss the crystalline state of the MC-AC sample as a good model for the ordered gel state. The spectrum (Figure 3D) of the MC-SC sample is the only one remaining; however, this spectrum shows evidence that more than one component is present because the C5 multiplet intensities in the 76–81 ppm region (a) by intensity belong to only one carbon and (b) by multiplicity and relative multiplet intensities do not seem to be in the ratio of small whole numbers (as one expects for a single unit cell). Assuming that two crystalline components are present, we attempted to separate³⁸ component spectra on the basis of the possibility that respective proton relaxation times, either rotating frame ($T_{1\rho}^{\text{H}}$) or longitudinal (T_1^{H}), were different in each region. T_1^{H} showed no contrast; however, $T_{1\rho}^{\text{H}}$ gave mild contrast. Owing to spin diffusion, if the shorter $T_{1\rho}^{\text{H}}$ encountered is more than a few milliseconds (true for this case), then component spectra, obtained in this way, will closely approximate the true spectrum of each component. Figure 4 shows component spectra based on $T_{1\rho}^{\text{H}}$ contrast. Spectra in Figure 4A,B, respectively, correspond to experimental spectra having proton spin-locking times of 0 and 8 ms prior to cross polarization. Spectra in Figure 4C,D are the component spectra derived from different linear combinations of Figure 4A,B. Spectra in Figure 4C,D are also scaled so that their added intensities correspond to the intensities in Figure 4A. Linear combinations used to generate Figure 4C,D are chosen on the basis of eliminating certain spectral regions without having them go negative. In this case, Figure 4C represents the major spectral component with about two-thirds of the total intensity, and on the basis of only this two-point decay, the longer $T_{1\rho}^{\text{H}}$ is 40 ± 4 ms whereas the shorter $T_{1\rho}^{\text{H}}$ is 21 ± 4 ms. The sample seems adequately described as having two regions, albeit more regions are possible if their $T_{1\rho}^{\text{H}}$ s are very similar. It is notable that the spectrum in Figure 4D seems to be missing the C6 resonance entirely; however, this is an artifact of the signal-to-noise ratio in Figure 4D that is not sufficient to identify the broad C6 contribution beneath the 66 ppm peak in Figure 4A. In contrast, the C5 resonance is intact in Figure 4D.

Figure 5 shows a comparison of spectra of the major components of MC-SC (Figures 5A and 4C are the same) and of the 2% DBS-in-benzene gel–solid (Figure 3B). Although the resolution in Figure 5A is much better than in Figure 5B, the mean shifts for each resonance group as well as the overall asymmetric shapes for the broader lines correspond well to one another. Hence, we

(35) Horii, F.; Hirai, A.; Kitamaru, R. *Polym. Bull.* **1983**, *10*, 357.

(36) Suzuki, S.; Horii, F.; Kurosu, H. *J. Mol. Struct.* **2009**, *921*, 219.

(37) Wu, X. L.; Burns, S. T.; Zilm, K. W. *J. Magn. Reson., Ser. A* **1994**, *111*, 29.

(38) VanderHart, D. L.; Perez, E. *Macromolecules* **1986**, *19*, 1902.

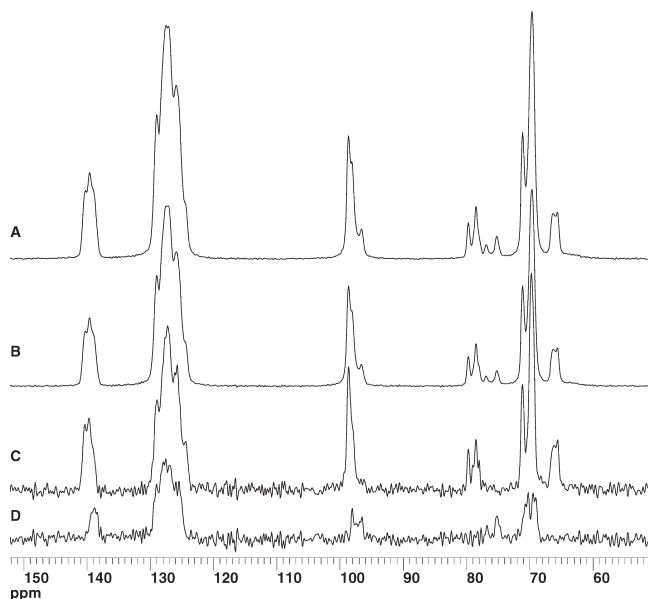


Figure 4. ^{13}C spectra of the MC-AC DBS sample (spectrum in Figure 3D) showing the separation of two coexisting crystalline regions. (A, B) Experimental CPMAS spectra with, respectively, 0 and 8 ms proton spin locking prior to cross polarization. The fact that rotating-frame proton relaxation times, $T_{1\rho}^{\text{H}}$, are different in the two regions allows one to take different linear combinations of A and B to generate the component spectra, C and D. This method preserves relative intensities within each component. Scalings of C and D are chosen so that $C + D = A$; thus, C has about two-thirds of the total intensity. The lack of observable C6 intensity in D is an artifact of the signal-to-noise level being inadequate for detecting the very broad C6 resonance seen in A and B.

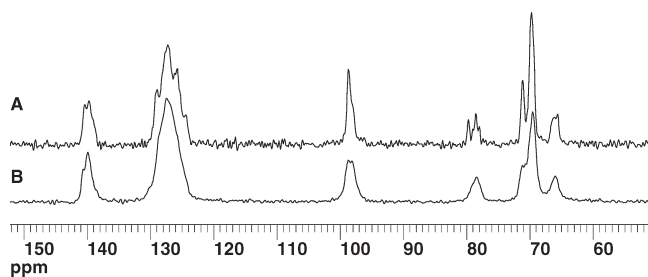


Figure 5. Comparison of (A) the major component of the MC-AC sample (Figure 4C) and (B) that of the 2% DBS-in-benzene gel–solid (Figure 3A). Aside from the poorer resolution in B relative to that in A, the strong correspondences in overall line shapes and shift positions rationalize the claim that the dominant crystal structure in this MC-AC sample is very similar to the packing in the gel state.

conclude that the dominant crystal structure associated with the slowly cooled DBS melt is the crystal structure that most closely mirrors the organization of DBS molecules in the gel–solid. On the basis of this result, we then attempted to apply different thermal posthistories to the MC-AC sample in order to optimize, via solid-state crystal transformation, the content of the crystal structure related to the gel. We were unsuccessful in finding a way to modify the ratio of the two crystal structures (i.e., once the annealing temperature exceeded 170 °C, transformation occurred, but always to the same ratio of crystal structures that the MC-SC sample had produced). This result, in turn, led us to suspect that this solid-state partitioning might be accompanied by the inability of the desired crystalline form to propagate without bounds. That notion, in turn, suggested that the two crystalline

forms might be mixed on a rather small scale. Therefore, we did a very crude spin diffusion experiment where the initial polarization gradient was developed on the basis of differing average T_{1xz} values. Results suggested that the two crystalline forms were well mixed on a distance scale of 20 nm. More details about annealing and the scale of mixing can be found in the Supporting Information.

Returning to the MC-AC sample, we also applied the $T_{1\rho}^{\text{H}}$ test for multiple components; however, we failed to find multiple components. Hence, the multiplicities seen in the spectrum in Figure 3E, especially in the 76–81 ppm region, likely indicate two magnetically inequivalent sites within a single unit cell. Such a conclusion is also supported by the approximately equal component intensities in this same region.

^{13}C Longitudinal Relaxation Times, T_1^{C} , at 25 MHz for Various Solid DBS Samples. We measured approximate T_1^{C} values at ambient temperature (22 °C) in several preparations because such measurements, when limited to the protonated carbons, are useful as a probe for identifying any molecular sites that deviate substantially from the average mobility. For DBS, sites of above-average mobility could, in principle, include the pendent carbons, C5 and C6, or, to a lesser extent, aromatic carbons that are subject to rotations or librations about the C7–C8 and C7'–C8' bonds. Because the main objective of these T_1^{C} measurements was to identify any such notable inhomogeneities in T_1^{C} from site to site, T_1^{C} measurements were typically based on only three or four points along the decay, and the T_1^{C} values cited are thus claimed to be accurate only to $\pm 20\%$ of their measured value. The cited times are those at which the signal has decayed to $1/e$ of its initial value. Also, we are not claiming strictly exponential decays. For any particular sample characterized by natural-abundance ^{13}C distributions, the longer decays tend to have some nontrivial, nonexponential contribution from ^{13}C – ^{13}C spin exchange with any faster-relaxing ^{13}C nuclei that lie within about 0.7 nm of those nuclei observed.³⁹ (For our natural-abundance samples with about 1.1% ^{13}C nuclei, such internuclear distances within 0.7 nm are statistically determined and show a wide variation.) As a consequence, the relaxation pathways for those carbons with slower intrinsic relaxation rates tend to be more strongly mixed with contributions from faster relaxing sites. Table 1 summarizes the T_1^{C} measurements for each spectral region for most of the spectra appearing in Figure 1; correspondences with spectral labels in Figure 3 are also given. The as-received sample has the longest T_1^{C} s, followed closely by most of the carbons in the MC-SC sample. The 2% DBS-in-benzene gel–solid also has relatively long (~ 100 s) T_1^{C} s. The main samples of note, in terms of displaying inhomogeneous T_1^{C} s, are the MC-AC sample and, to a lesser extent, the MC-SC samples. The primary sites exhibiting motional inhomogeneity are the hydroxycarbons, C5 and C6. The most notably short T_1^{C} is associated with C6, whose downfield component in the spectrum in Figure 3E and broad bases in the spectra in Figure 3D,F provide sharp contrast in T_1^{C} relative to those of other sites in the molecule. In fact, in Figure 3E,F, C6 possesses T_1^{C} s short enough to indicate corresponding correlation times for the molecular motion of the hydroxymethylene protons within about an order of magnitude of the theoretical T_1^{C} minimum value⁴⁰ ($T_{1(\text{min})}^{\text{C}} = 20$ ms at a correlation time of 5×10^{-9} s for an isotropically rotating CH_2 carbon at 25 MHz). In other words, the longest correlation time that could account for the observed relaxation

(39) VanderHart, D. L. *J. Magn. Reson.* **1987**, *72*, 13.

(40) Abragam, A. *The Principles of Nuclear Magnetism*; Oxford University Press: London, 1961; Chapter 8.

Table 1. Approximate T_1^C Values (25 MHz) Associated with the Indicated Spectral Regions for DBS in Various Solid-State Forms^a

sample/spectrum ^b	T_1^C (s) for given carbons and chemical shift ranges (ppm)					
	C6 (64–68)	C1–C4 (68–73)	C5 (76–81)	C7, C7' (97–101)	C9–13, C9'–13' (124–131)	C8, C8' (138–140)
2% benz-gel–solid/3A	120	100	120	110	80	110
as received/3C	390	330	390	390	270	470
MC-SC/3D ^c	250 < 1 ^d	> 110	290	> 250	> 100	> 290
MC-AC/3E (nearly dry)	5.1 and 0.15 ^d	75	88 and 26 ^e	95	74	115
MC-AC/3F (aged 15 days)	9.3 and 0.12 ^d	80	100 and 47 ^e	105	90	125
MC-AC (75% RH)	3.3 and 0.25 ^d	46	54 and 19 ^e	66	52	92

^aStandard uncertainties are $\pm 20\%$ of the given values unless otherwise indicated. Oxygen is present during these measurements. ^bSpectral associations, when given, refer to spectra in Figure 3. ^cThis sample has two phases where the minority phase has shorter T_1^C s; however, the given T_1^C s are associated with the majority phase (i.e., the phase related to the gel structure). An exception is the lower value for C6 corresponding to the minority phase. For spectral regions where signals from the two regions overlap (Figure 2), only the lower limits of T_1^C are indicated. ^dUpper T_1^C corresponds to a narrower resonance, and lower T_1^C corresponds to the broader underlying resonance. ^eUpper T_1^C is for the most downfield line of the range, and lower T_1^C is for the adjacent line.

time would be near 10^{-7} s. At the remaining C6 sites in the MC-AC samples, T_1^C s are at least an order of magnitude longer, indicating either slower motions or more restricted amplitudes of motion. Comparatively, the adjacent C5 carbons show much more restricted motions (i.e. one C5 site has a T_1^C comparable to that of the remaining sites; the other has a T_1^C of about one-half or one-third of the average). The MC-SC sample also shows significant motional heterogeneity; however, in this case, all of the C6 carbons in the minority phase seem to be motionally active whereas those in the majority phase are very rigid. In summary, for the T_1^C data in Table 1 we draw two main conclusions: (a) except for the MC-AC sample and the minority crystalline phase of the MC-SC samples, all remaining DBS solids investigated, including the gel–solids and the majority phase of the MC-SC samples, feature relatively rigid molecules where that rigidity extends to the hydroxycarbons, C5 and C6 and (b) the MC-AC sample shows heterogeneous and high local mobility for about half of the hydroxymethylene carbons and modestly high mobility for the other half of those carbons, whereas the rest of the molecule is significantly more rigid. There is a strong suggestion that the crystalline state of the MC-AC sample and the minority crystalline state of the MC-SC samples are characterized by hydrogen bonds at C6, which, if they exist, are relatively (and, for MC-AC, inhomogeneously) weak compared to much stronger hydrogen bonds in the remaining samples, including all gel–solids and the majority phase of the MC-SC samples.

Notably absent from Table 1 are measurements made directly on in situ gels. This is partially due to the fact that the sensitivity is not adequate to detect, with a good signal-to-noise ratio, the ^{13}C spectrum of a sample having only about 2% gel–solids. Moreover, we do not have liquid-tight rotors for use with MAS. As mentioned in the Experimental Section, we believe that the dried 2% DBS-in-benzene gel–solid is a good model for the in situ gel–solid, unless benzene somehow permeates DBS in the in situ gel–solid.

We also investigated the gel in situ to get some independent verification (a) that the DBS molecules were quite rigid and (b) that, in the gel state, the solvent was not incorporated into the lattice. To do this, we turn to proton NMR, which, compared to ^{13}C NMR, offers a large increase in sensitivity at the expense of spectral resolution.

Rigidity of the in Situ Gel–Solids and Demonstration That Solvent Does Not Infiltrate the Gel Structure. Table 2 gives 300 MHz proton longitudinal relaxation times, T_1^H , for several solid samples, including those for three in situ gelled samples in sealed tubes with deuterated solvents (acetone- d_6 and benzene- d_6). For these in situ samples, the T_1^H s listed are quite long and correspond only to the broad nonliquid component. T_1^H

Table 2. Longitudinal Proton Relaxation Times, T_1^H , at 300 MHz and Ambient Temperature for DBS in Different Samples under Various Measurement Conditions

DBS sample	O ₂ present?	dried?	T_1^H (s) ^b
2.1% in acetone- d_6 , sealed tube ^a	N	N/A	31 (5)
1.1% in acetone- d_6 , sealed tube ^a	N	N/A	32 (5)
2.1% in benzene- d_6 , sealed tube ^a	N	N/A	50 (7)
120 °C-dried gel–solid from	Y	Y	5.3 (6)
2.0% DBS-in-benzene	N	Y	20 (2)
120 °C-dried gel–solid from	Y	Y	2.8 (3)
2.3% DBS-in-acetone	N	Y	18 (2)
as received	Y	N	13.6 (8)
	N	Y	87 (5)
rapidly melted and air cooled	Y	N	9 (1)
(MC-AC)	N	Y	9 (1)
melted and cooled at 3 °C/min	Y	N	30 (3)
(MC-SC)	N	Y	70 (4)^c

^a T_1^H of the solid component only. ^bStandard uncertainties of measurements are shown in parentheses in units of the least-significant figure. ^cWe looked for the nonexponential decay with two components but was not found in this sample because two domains were identified from $T_{1\rho}^H$ measurements.

values for the dried solids, in the absence of oxygen, are within a factor of 2 or 3 of those of the other oxygen-free, strongly hydrogen-bonding solid forms of DBS. An exception is the MC-AC sample with the shortest oxygen-free T_1^H (9 s), which we attribute to the influence of the short intrinsic relaxation time of the very mobile, well-distributed hydroxymethyl protons identified in Table 1. Again, just as reflected in the T_1^C data of Table 1, the as-received DBS sample has the longest T_1^H and therefore seems the most rigid; again, the second most rigid is the MC-SC sample. A few T_1^H s for samples in the presence of atmospheric paramagnetic oxygen are also included. Oxygen is seen to cause a significant shortening of T_1^H except for the MC-AC sample. If we made the assumption that oxygen was excluded from the crystalline lattice of the solids and exerted its influence only on available surfaces in the solids, then one might surmise that the highest surface area belonged to the 2.3% DBS-in-acetone gelled solid, followed by the 2.0% DBS-in-benzene gelled solid and the as-received sample.

As a final qualitative deduction from Table 2, we note that the incorporation of any solvent into the in situ gel–solid phase, with either acetone or benzene present, seems very remote. For in both the in situ and dried forms of the oxygen-free 2% DBS-in-benzene samples, the T_1^H of the former exceeds that of the latter. Moreover, for the proton spectrum of the in situ 2% DBS-in-benzene sample, aside from some weak high-resolution contributions from residual solvent protons, residual DBS in solution, and traces of water, all of the broad contributions to the proton spectrum gave

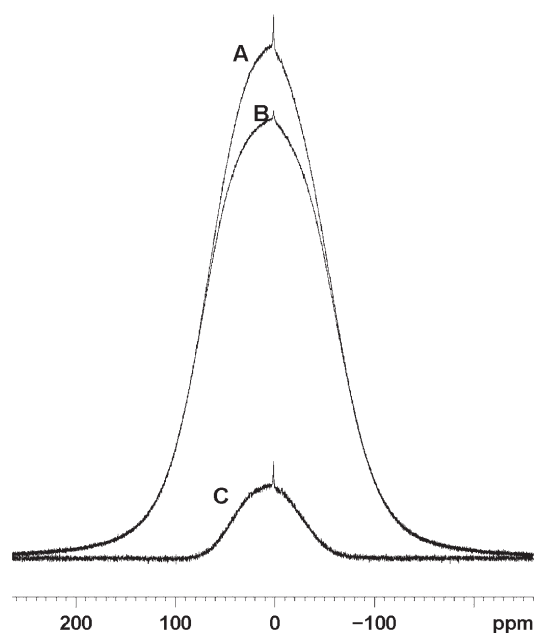


Figure 6. Overlay of proton Bloch-decay spectra (300 MHz) for the 2% DBS-in-benzene dried gel–solid (A) and the dried, as-received (B) samples. B is scaled so that the difference spectrum, C, is nowhere negative. The intensity of C is 7% that of A. Small, sharp resonances are artifacts.

a line shape (Supporting Information) indistinguishable from that of the corresponding dried gel–solid. If there were solvent in the in situ gel–solid, then the expectation, counter to what is observed, would be that both line widths and T_1^H for the in situ sample should decrease relative to those for the dried sample, owing to the solvent-induced mobility of the DBS molecules. Note that this argument would not necessarily counter the speculation⁷ that fibrils could be hollow as long as the walls of the fibril are made up of largely immobilized molecules.

Molecular Mobility at the DBS Fibril Surface. In this section, we are interested in the existence and location, morphologically, of molecules in the gelled solids that have modestly enhanced mobility relative to that of the average molecule in the as-received sample. Recall that molecules in the as-received sample, according to both ^{13}C and ^1H relaxation measurements, are quite rigid. Moreover, molecular packing as judged by the ^{13}C spectra is similar to that of the gelled solids. The notion that the lateral growth of the fibrils is self-limiting (i.e., the energy of molecular deposition on the surface is decreasing with increasing fibril diameter) could lead to the expectation that there is a gradient of increasing mobility as one moves from the fibril core toward the fibril surface. However, such an increase might also occur because molecules on a surface are not completely surrounded by neighboring molecules. In any case, there are good reasons to expect that DBS molecules on the fibril surface might not be as rigid as molecules buried within the fibril.

In Figure 6, 300 MHz Bloch-decay spectra are compared for the 120 °C-dried, 2% DBS-in-benzene sample (Figure 6A) and the dried as-received sample (Figure 6B). The scaling of these spectra is chosen so that the difference spectrum (Figure 6C) is nowhere negative. The integral of Figure 6C is 7.8% of that of Figure 6A, and the respective line widths (full widths at half height) are 40.0 ± 0.7 , 43.3 ± 0.7 , and 22.5 ± 1.0 kHz for Figure 6A–C. The main deduction from Figure 6 is that, compared to the dried, as-received sample, the 120 °C-dried, 2% DBS-in-benzene sample has a slightly narrower overall line width, which involves a nontrivial

motional narrowing for a minimum of 7.8% of the total number of protons. (We emphasize “minimum” here because the motional narrowing might also involve less narrowing for a greater percentage of protons.) That is why we will presently try to assay the spatial inhomogeneity of this mobility gradient. Before doing this, however, we must be certain that this slightly narrowed component cannot arise from residual benzene that is trapped and largely immobilized in the lattice. The absence of such trapped benzene, as expected by the relaxation arguments for the in situ samples in the last section, is shown directly by the identical aromatic/aliphatic proton-intensity ratios in CRAMPS spectra of the as-received and the 2% DBS-in-benzene samples (Supporting Information). Therefore, in Figure 6, the line narrowing seen in the Bloch-decay spectrum of the 120 °C-dried 2% DBS-in-benzene sample can be attributed to the increased motion of some (or all) of the DBS molecules.

The foregoing conclusion raises the question of whether the observed increased mobility in these dried fibrils can be associated with molecules on the fibril surfaces. If so, the fraction of mobile molecules reflected in the spectra of the dried gel–solids might give some indication of fibril size. From our TEM images, lateral fibril dimensions for the as-received and the 120 °C-dried 2% DBS-in-benzene sample are, respectively, 50–70 nm and 12–21 nm (i.e., fibrils for the latter sample are approximately 2.5 to 6 times smaller than for the as-received sample). Surface-to-volume ratios should vary inversely with the diameter ratio. Therefore, the 120 °C-dried 2% DBS-in-benzene sample should have a fraction of surface molecules that are at least a factor of 2.5 times larger than in the as-received sample.

We therefore employed a series of experiments intended to test the hypothesis that the observed additional mobility of the 2% DBS-in-benzene sample, relative to that of the as-received sample, arises mainly from surface sites on the fibrils. In these experiments, we first show that faster T_{1xz} decay rates are associated with the more mobile component of the Bloch-decay spectrum. Then, we do a T_{1xz} - T_{1xz} -SD spin diffusion experiment and use those results to estimate a fibril diameter, assuming that excess mobility can be associated with fibril surfaces. The agreement of that estimated diameter with that observed by TEM is then taken as verification of the excess mobility at the surface.

The first experiment demonstrates the correspondence between greater mobility and shorter T_{1xz} 's. In Figure 7, two types of truncated T_{1xz} decays for the 120 °C-dried 2% DBS-in-benzene sample are compared. That of the whole sample is given in Figure 7A. In Figure 7B, the T_{1xz} decay associated with a T_{1xz} - T_{1xz} -SD experiment is shown. (This is the T_{1xz} response after a preparation consisting of 14 ms of T_{1xz} irradiation followed by a very short spin diffusion time, t_{sd} , of 20 μs , during which very little spin diffusion occurs.) The decay in Figure 7B captures mainly a longer decaying component after a substantial amount of the faster decaying component has previously decayed away. Related Bloch-decay spectra (nonspinning samples) corresponding to Figure 7A,B are given in Figure 7C,D, respectively (i.e., Figure 7C is the equilibrium spectrum, and Figure 7D is that acquired following 14 ms of T_{1xz} decay and a t_{sd} of 20 μs). For purposes of ease of comparison, Figure 7B,D are vertically scaled, respectively, to coincide with the longer decay of Figure 7A and the wider line width component of Figure 7C. For clarity of display, full T_{1xz} decays and Bloch-decay line shapes for the as-received sample are not shown; however, those data are very close to Figure 7B,D indicating that the 14 ms of T_{1xz} decay has strongly reduced the relative intensity contribution from the more mobile protons. Hence, the correspondence between mobile components in the Bloch-decay spectrum and shorter T_{1xz} is established, and

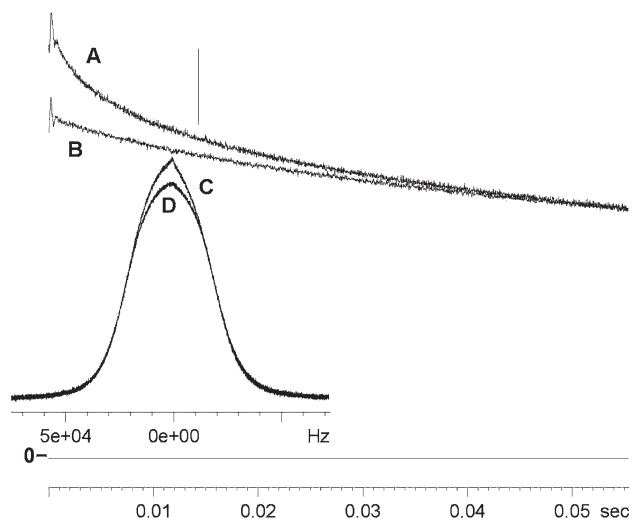


Figure 7. Proton NMR data (300 MHz) demonstrating that for a nonspinning, dried, 2% DBS-in-benzene gel–solid sample the faster relaxing protons in a T_{1xz} experiment are associated with the narrower component (Figure 7) of the Bloch-decay line shape. (A) The first 57 ms of T_{1xz} decay for M_0 magnetization; the signal level corresponding to “zero” is indicated just above the time axis. (B) Decay (57 ms) of the longer T_{1xz} component, isolated in a T_{1xz} - T_{1xz} -SD experiment with a 14 ms T_{1xz} preparation and a short, 20 μ s spin diffusion time. B is vertically scaled to have equal intercepts with A at 57 ms. C and D are respectively Bloch-decay spectra associated with initial magnetizations in A and B, where D is vertically scaled such that C and D are nowhere negative. Line shape D is identical to that of the as-received sample (Figure 6B).

we can move on to test whether the spin diffusion behavior, connecting the more rigid and more mobile protons, is consistent with mobility mainly residing at the fibril surface.

The second experiment in this set is again a T_{1xz} - T_{1xz} -SD experiment in which a polarization gradient, based on differential mobility, is set up and then allowed to dissipate via spin diffusion. Results are used to estimate a fibril diameter. The gradient dissipation (equilibration) time, thus obtained, is then converted to a distance scale by a calculation that invokes a proper spin diffusion constant. As a matter of perspective, from a comparison of Figure 7A,B, the faster T_{1xz} component in the dried 2% DBS-in-benzene sample comprises 20–25% of the total proton spins. In addition, if the mobile protons were intimately mixed with more rigid protons on the same or adjacent molecules, then full equilibration would be expected in 1 or 2 ms. However, if the more-mobile component were sequestered in larger domains, then full spin equilibration would take longer, depending on the domain sizes (or fibril diameters).

Figure 8 shows data obtained from the T_{1xz} - T_{1xz} -SD experiment as a function of t_{sd} . The ordinate in Figure 8 is an arbitrarily normalized quantity that is proportional to the absolute magnitude of the departure of the polarization of either the faster- or slower-relaxing component from samplewide equilibrium.

To model this spin diffusion behavior, we performed a spin diffusion calculation by assuming (a) that the DBS gel–solid consisted of solid rods of diameter d having a more-mobile layer of thickness Δd on the surfaces of the rods, (b) that the 14-ms T_{1xz} preparation produces a step function in the polarization at the core-layer interface, and (c) that the spin-diffusion constant for the DBS molecules is $0.6 \text{ nm}^2/\text{ms}$. The fit shown is for $d = 18.8 \text{ nm}$ and $\Delta d = 1.15 \text{ nm}$. In this case, the surface layer comprises about 25% of the rod volume, consistent with the data. The fit is reasonable, albeit not perfect. Nevertheless, we conclude that the

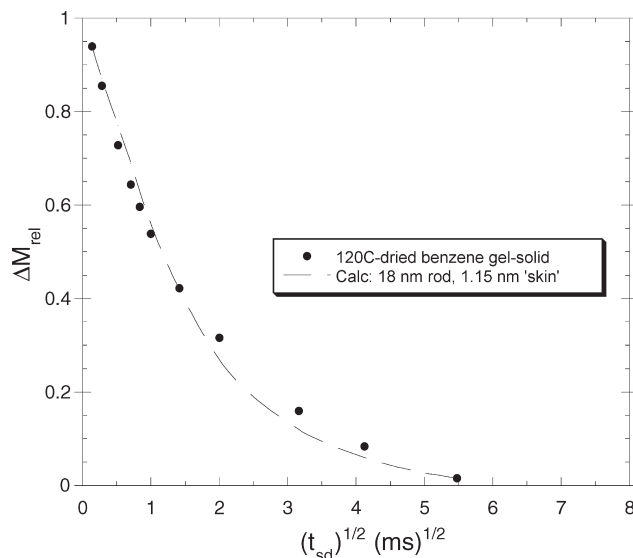


Figure 8. Spin diffusion plot (dried 2% DBS-in-benzene sample) for the T_{1xz} - T_{1xz} -SD experiment whose data is sampled in Figure 7. The dashed line is a computational fit for spin diffusion in isolated rods having a surface layer with a higher mobility and a shorter T_{1xz} . The legend indicates the rod diameter and skin thickness for the calculation. The variable, ΔM_{rel} , is a quantity that is proportional to the magnitude of the deviation of either the faster- or slower-relaxing component from samplewide spin equilibrium.

inferred diameter of the fibrils is in good agreement (12–21 nm range) with the TEM results, thereby strongly supporting the morphological model of a surface for the dried gel fibrils where the mobility is significantly higher than the mobility that typifies its core. Incidentally, the Δd parameter also fits the model reasonably well in that a 1.15 nm distance would correspond to 1 or 2 thicknesses of DBS molecules, depending on the orientation of those molecules with respect to the surface. We recognize that the good agreement between TEM-determined and NMR-inferred fibril diameters depends modestly on our choice of diffusion constant. In our case, we chose the spin-diffusion constant based on literature estimates;^{41,42} also, chronologically, a determination of fibril diameter by NMR preceded the TEM result.

Ambient-Temperature Kinetics of Gelation of in Situ 1.43% DBS-in-Acetone and 2.05% DBS-in-Acetone and Residual Levels of Dissolved DBS in Acetone and Benzene. The concentration of DBS in solution before, during, and after an extended period of gelation can be measured quantitatively by NMR provided gelation occurs relatively slowly. For those cases where gelation is rapid, one can follow only longer-term changes in DBS concentration. For a well-gelled sample, one can also measure the integral of the dissolved DBS against that of the solid DBS, given the large proton line width differences between the two states. Thus, it is found that after at least 3 days of gelation at $295 \pm 0.5 \text{ K}$ the solubility of DBS in a sample originally 2.0% DBS-in-benzene- d_6 is less than 0.1% by mass. In contrast, it is $0.65 \pm 0.03\%$ by mass in a gel that was originally 2.05% DBS-in-acetone- d_6 . Thus, at ambient temperature, DBS is considerably more soluble in acetone than in benzene.

To study the kinetics of formation, we chose acetone as the solvent with which to study DBS gelation because DBS gels too quickly form benzene and because the residual levels of DBS in

(41) Clauss, J.; Schmidt-Rohr, K.; Spiess, H. W. *Acta Polym.* **1993**, *1*, 44.

(42) VanderHart, D. L.; McFadden, G. B. *Solid State Nucl. Magn. Reson.* **1996**, *7*, 45.

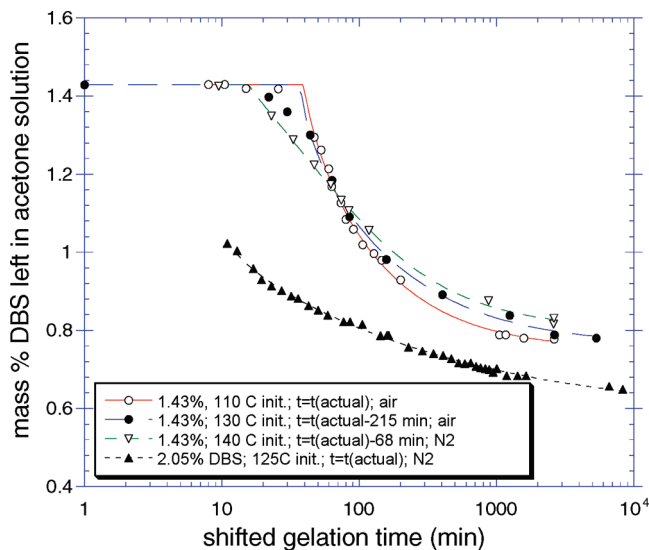


Figure 9. Concentration of DBS remaining in acetone solution as a function of gelation time at 22 °C for the 1.43% DBS-in-acetone and 2.05% DBS-in-acetone samples. Three different gelation cycles were run sequentially on the same 1.43% sample (see legend for initiation temperatures, time shifts used for plotting comparisons, and atmospheres above the sealed samples); the sequence in the legend is also the chronological order. The gelation time, t , begins when DBS is removed from the high-temperature bath and is immediately loaded into the NMR probe with its air flow. Equation 1 is used in the fits, and the parameters determined are given in Table 3.

acetone solution provide reasonable sensitivity for monitoring small changes in concentration.

We prepared a sample, which by mass was 1.43% DBS-in-acetone- d_6 . This sample was initially frozen in liquid nitrogen on a vacuum line, pumped down, backfilled with the partial pressure of air, and sealed. The kinetics of gel formation was studied three times for this sample. First, an initiation temperature of 110 °C was used. The second run was preceded by an initiation temperature of 130 °C. Prior to the third run, the sample was reopened, placed on a vacuum line, taken through two cycles of freeze-pump-thaw, and sealed again under nitrogen. This oxygen-free sample was then initiated at 140 °C. A plot of the mass percent of DBS in solution versus log(gelation time) is included in Figure 9. Gelation kinetics in the three runs on the 1.43% sample are similar to one another with the exception (see legend) that the incubation period prior to gelation is quite unpredictable, varying from about 20 min to about 4 h with no consistent correlation with the initiation temperature or atmosphere. Also included in Figure 9 are data from the 2.05% DBS-in-acetone- d_6 sample after initiation at 125 °C. In this case and owing to the higher concentration, we were unable to capture the onset of gelation, hence only the later stages of gel growth can be monitored. Parallel to observations on the 1.43% sample, there is a slow, steady loss of DBS from solution with time that is evident when the DBS solution concentration is plotted as a function of logarithmic time. In this article, we will qualitatively discuss the gelation behavior after the onset of gelation and refrain from speculating on why the incubation time varies.

The visual appearance of the gels examined by NMR varied to some extent (Figure S5 in the Supporting Information). None was completely clear optically. The 1.43% sample generally showed visible, wispy, whitish regions occupying minor portions of the volume. To us, the most likely explanation for these visible regions is that the density of the gel varied somewhat across the sample. However, it is certainly not true that the clear regions

contained no gel because these samples did not flow at all when tipped on their sides. In all cases, the appearance of the wispy regions was stable from the time of formation onward (i.e., the slow evolution of concentration did not arise from a settling of the regions of higher gel density into the regions of the NMR coil).

Discussion

Nature of the in Situ Gel Structure. It seems clear that the DBS gel–solid in its in situ form is organized into a rigid structure, and depending on the solvent, there can be quite a variation in the amount of DBS remaining in solution. The in situ T_1^H s of Table 2 and the Bloch-decay line width of Figure 7 (and Figure S3 in the Supporting Information) strongly suggest that the DBS associated with the fibrils is very rigid; moreover, solvent is not in the lattice of the DBS. Hence, we have more confidence that the gel–solid, especially that isolated and dried from the benzene gel (where DBS precipitation during drying is minimal), is a good representation of the in situ gel–solid.

The dried 2% DBS-in-benzene gel–solid has other characteristics besides the relatively rigid solid-state organization. First, the T_1^C s for both hydroxyl carbons are quite long, indicating that hydrogen bonding at C5 and C6 is strong. This supports the notion that the formation of strong hydrogen bonds is an important consideration in determining the solid-state gel structure. That structure stands in distinction with respect to the crystalline structure formed by more rapid air cooling from the melt at 230 °C, and we digress to discuss this MC-AC sample.

Just below 230 °C, during melt crystallization, hydrogen-bonding interactions do not strongly dominate the thermal energies. The consequence is that the crystal structure nucleated at higher temperatures can be strongly influenced by considerations other than hydrogen bonding. The MC-AC structure, although relatively well ordered judging by the good spectral resolution for most of the ^{13}C resonances, exhibits hydrogen bonding, especially at C6, that is both inhomogeneous and weak. We were also particularly interested in why there was a spectral change with time in the ^{13}C spectra of the MC-AC sample (Figure 3E,F). We followed spectral changes over a period of about 1 year; however, these changes were continuous but not monotonic. In particular, we found that the changes related to the average relative humidity and not to the time of aging. In fact, sample drying in vacuum was found to return the sample to its initial state (spectrum in Figure 3E). The pervasiveness of the spectral changes at C5 and C6 (broadening and continuous, humidity-dependent shifts for the upfield doublet components in Figure 3F relative to those in Figure 3E) indicated that, in spite of the high crystallinity of this sample, water of hydration had access to at least half of the C6 sites and the residence times for the water at any C6 site were much shorter than 1 ms. (This latter conclusion is based on the observation that, at each humidity level investigated, there is a uniform, chemical-exchange-averaged shift describing the mobile C6 sites even though the amount of water is not adequate to populate all sites uniformly.) Hence, this DBS crystal structure, formed by air cooling from the melt, is sufficiently open (possibly of lower density as well) to allow water access into its crystal structure. Notably, the crystal structure of the MC-AC sample is deemed to be monolithic (not mixed) on the basis of the relative intensities and the lack of $T_{1\rho}^H$ contrast. Corresponding spectral changes upon hydration at nonhydroxy carbons are noticeable in some cases (i.e., near 70 ppm and from 126 to 128 ppm) but are not particularly dramatic, thereby confirming the expectation that hydroxy sites would be points of attraction for water, especially if those sites exhibited weak H bonds in the dry structure. The

strength of the broadening at C6 relative to that at C5 is also an indication that at least half of the C6s are strongly interacting with the water.

A final comment on the MC-AC sample regards qualitative relative molecular mobilities and is based on Table 1. Again, T_1^C 's for C6 show strong excess mobility for about half the sites with the other half of the sites showing intermediate mobility. C5 also shows differential mobility, albeit the differences are much less dramatic than those at C6. In fact, it is possible that the intermediate mobility inferred for C5 mainly reflects contributions from motions of the hydroxymethyl protons at C6 rather than reorientations of the H-C bond at C5. All other nonhydroxy carbons in the MC-AC sample show T_1^C 's that are only mildly reduced from those seen in other samples. However, we do not insist on a significant increase in the average mobility for these sites relative to that for the same sites in other DBS samples in view of the fact that paramagnetic oxygen, O_2 , might contribute slightly to T_1^C , given that water can infiltrate the crystal.

In summary, for the MC-AC sample, the crystal structure is sufficiently open to allow reversible hydration for about half of the C6 sites (with correspondingly high mobility exhibited by these hydroxymethyl groups) and intermediate mobility for the other half of the C6 sites. This crystal structure exhibits weak H bonds at C6 and, in that sense, stands in sharp contrast to the gel-solids, including the as-received sample. The latter samples are characterized by uniformly long T_1^C 's, implying strong H bonds that inhibit the motion of the hydroxymethyl groups at C6.

Returning to the structure of the gel-solid, we have also identified some heterogeneity in mobility within the dried fibrils (Figures 7 and 9) and have associated the excess mobility with the fibril surface. Such a mobility gradient would logically be expected if lateral fibril growth were energetically limited because of the diminishing affinity of DBS for the outer, surface sites. Alternatively, such a gradient might also be explained by the fact that a molecule at the surface of a fibril would have fewer lattice constraints than one buried in the interior. We cannot choose one argument over the other at this point. (Incidentally, the fraction of "surface" protons involved precludes the possibility that when the gel is dried the fibril surfaces may become "coated" with a less-organized layer of DBS that would not normally have been immobilized at the surface when benzene was present. We dismiss this latter possibility on the basis of the fact that more than 95% of the DBS is in the fibrils prior to the beginning of solvent removal.)

Besides the characteristics of rigidity, strong hydrogen bonding, and enhanced surface mobility, the lack of good resolution in the ^{13}C spectra of the dried gel-solids offers a final insight into the nature of the gel-solid. The following remarks are very qualitative and support the notion that the DBS fibril lacks a well-defined unit cell. First, the finite lateral size of the crystallites can give rise to line broadening owing to the fact that the variation in intermolecular environments produces a corresponding variation in the chemical shift including differences associated with surface sites. However, for a crystallite whose lateral dimension is close to 20 nm, the majority of the molecules have at least two molecular layers of intermolecular constraints. Thus, the expectation is that the interior resonances ought to be quite sharp. As a case in point, for cellulose fibrils from certain algae with an approximate diameter of 20 nm, the resolution is both excellent relative to that of cellulose fibers with diameters in the 3–6 nm range⁴³ and approaches that of chemically related sugars of a much larger crystallite size. Second, broadening may arise from molecular dynamics, particularly that having frequency components in the

midkilohertz region.^{33,44} However, for the gel-solids, $T_{1\rho}^H$'s, which are sensitive to the presence of such motions, are in the range of tens of milliseconds, hence such broadening should be minimal. The Bloch-decay proton line shapes and the T_1^C 's of the gel-solids also support a picture of low molecular mobility. Finally, broadening associated with anisotropic bulk magnetic susceptibility³³ can exist, especially when the molecular structure incorporates aromatic groups, as DBS does. Considering the degree of resolution seen in the spectra in Figure 3E,F, where crystalline regions with packing similar to that of the gel-solids exist, one might logically expect that the susceptibility broadening seen in the MC-AC samples would be comparable to that in the gel-solid samples. Clearly, the MC-AC samples have a resolution that is greatly superior to that seen in the spectra in Figure 3A,B. Hence, variations in resolution in Figure 3 strongly suggest the lack of a uniform unit cell in the gel-solid structure and probably in the as-received structure as well. This is consistent with the notion (but not conclusive proof) that the gel-solid is a helical fibril exhibiting limited lateral growth, where the helicity, as discussed in the Introduction, is not contained within a unit cell and where intermolecular interactions cannot be preserved as the lateral dimensions change.

A final point regarding DBS structures relates to the similarity of crystal partitioning found for the slow-cooled, melt-crystallized sample of DBS (MC-SC) as well as the annealed MC-AC-170 and MC-AC-ramp175 samples. In each of these samples, the same mixture (approximately 2:1) of two crystalline forms is produced, with the major form strongly resembling the structure of the gel-solid.

There is one thing that remains a bit puzzling about the uniformity of each of these latter samples, especially in the context of realizing that these two crystalline forms are intimately mixed on a distance scale of no more than 11 nm, assuming an idealized lamellar morphology (or approximately 20 nm assuming a rod/matrix morphology).⁴² Recall that the latter is the upper limit found for the summed distance across both crystalline domains. (Also, if the domains are strongly anisotropic in shape, then this distance corresponds to the sum over the shortest path across domains.) However, the superior spectral resolution seen in these samples relative to that in the gel-solids and the as-received sample would suggest ordering more typical of a true unit cell. However, our inability to find conditions that alter the ratio of the two phases in the MC-SC sample is noteworthy. One wonders whether the reason that the major phase quits growing is similar to the rationale for the limited growth of the gel fibrils. However, because we have argued that poorer resolution in the fibrils is indicative of the lack of a crystalline unit cell, it would be surprising if the growth limitation would be associated with a legitimate unit cell. The fact that the major crystalline phase in the MC-SC sample possesses a spectrum very similar in chemical shift to that of the gel-solids strongly suggests that crystal packing in the major phase is very similar to the packing in the gel-solids. Recall also that TEM shows that the dried gel fibrils and the as-received material have lateral dimensions that are comparable to or substantially exceed 11–20 nm. Then how can one account for better spectral resolution for a smaller domain with similar packing? Speculative answers include the following two possibilities: (1) Broadening from anisotropic magnetic susceptibility perturbations associated with the orientation of nearest-neighbor fibrils is very important and that, in the solid-solid crystal transformation that is associated with the MC-SC samples, a much more uniformly oriented array of nearest neighbors results

(43) Earl, W. L.; VanderHart, D. L. *Macromolecules* **1981**, *14*, 570.

(44) Maricq, M. M.; Waugh, J. S. *J. Chem. Phys.* **1979**, *70*, 3300.

Table 3. Parameters Used in Fitting Equation 1 to the Time Dependences of the Solution Concentration, $c(t)$, of DBS in Acetone during Gelation at 22 °C for Various Initial Concentrations and Initiation Temperatures^a

c_o (%) ^b	initial T (°C) ^c	characteristic time t^* (min)	c_∞ (%) ^b	incubation time, t_o (min) ^d	ϕ
1.43(1)	110(3)	44(3)	0.76(5)	39(2)	0.90(6)
1.43(1)	130(4)	69(7)	0.78(2)	233(5)	1.07(15)
1.43(1)	140(4)	69(5)	0.78(1)	85(3)	0.76(5)
2.05(2)	125(4)	0.4(1)	0.58(2)	5.7(8)	0.30(2)

^a Uncertainties are expressed in parentheses in units of the least-significant figure and represent one standard deviation. ^b c_o and c_∞ are, respectively, the initial DBS concentration in the fully dissolved state and the final “equilibrium” concentration presumed to exist from the mathematical model. ^c Concentrations are expressed as mass percentages of DBS in acetone solution. ^d Figure 9 for the 1.43% samples employs times that are shifted from true times in order to facilitate a comparison of gelation rates. Corresponding incubation times vary widely.

in lines with much less broadening from nearest neighbors, hence lines narrower than those of the gel–solids. (2) The solid–solid transition reduces or eliminates helical twisting so that, especially for smaller domains, unit cell descriptions become better approximations, strain buildup is strongly reduced, and spectral resolution is thereby improved. However, this leaves the question of why such low-strain domains do not continue to grow. Perhaps relatively high nucleation densities then play some role in limiting growth. In any case, suffice it to say that, although intriguing, we do not fully understand the nature and seeming stability of the mixed crystalline states in the MC-SC, MC-AC-170, and MC-AC-ramp175 samples. However, there may be other thermal cycles or different combinations of solvent/temperature (e.g., ethylene glycol at 100 °C⁴⁵) that can be found that would result in a different structure or partitioning.

Kinetics of Gel Formation. A striking aspect of the gelation process is the very slow decrease of the DBS concentration in solution at long times (Figure 9). We sought a mathematical description of this behavior. (The motivation for this description, principally that of an assembling system under diffusion-controlled conditions, can be found in the Supporting Information.) Figure 9 shows a fit of our data to the resulting power-law equation

$$c(t) - c_\infty = (c_o - c_\infty) \left\{ 1 + \left(\frac{t - t_{\text{gel}}}{t^*} \right)^\phi \right\}^{-1} \quad (1)$$

where t is the time starting from when the solution begins to cool in air. Quantities c_o , $c(t)$, and c_∞ refer to concentrations of DBS in acetone solution before the onset of gelation (c_o), at time t (i.e., $c(t)$), and after infinite gelation time (c_∞). The fitting parameters, t_{gel} and t^* , respectively refer to the onset (or incubation) time for gelation and a “characteristic time” for the gelation process itself, once gelation begins. Finally, ϕ is a characteristic exponent that characterizes the long-time variation of $c(t)$.

In Figure 9, it can be seen that eq 1 does an excellent job of fitting the longer-time behavior, although it is not very good at capturing the earliest stage of gelation or at predicting the induction period. (Incidentally, the fitting program we used simply defined $c(t)$ to take the value of c_o for $t < t_{\text{gel}}$, ignoring the undefined nature of x^ϕ when x is negative.) Table 3 gives the fitting parameters associated with the data shown in Figure 9. We are most interested in the slow evolution in the DBS concentration at longer times and how this might relate to DBS organization. Although we believe that it is very useful to have an equation that well describes the aging-related concentration evolution of the gel, nevertheless we have chosen to shift to the Supporting Information most of our comments about (a) the motivation for invoking eq 1, (b) other detailed NMR observations related to the gelation process, and (c) possible underlying processes responsible for the slow reduction in DBS concentration in solution at longer times.

We made this decision mainly to shorten the article, recognizing that the justification for the use of eq 1 and the interpretation of the fits in terms of likely mechanisms of aging involve more speculative thinking. For example, the following two items contribute uncertainty to the fundamental applicability of eq 1. First, eq 1 describes a wide range of phenomena, hence it does not easily suggest a specific underlying mechanism. Second, we are not sure that the slow, longer-time changes are dominated by the same thermodynamic/kinetic processes that dominate the formation of the gel. The formation rate (much faster for the 2.03% than for the 1.43% sample), for example, dictates acceptable ranges for c_∞ and ϕ . One can see significant changes in these parameters for the two concentrations in Table 3, even though those differences were surprising to us within our understanding of the model. Thus, we present eq 1 as a starting point to be either supported, modified, or discarded on the basis of future experimental data.

In spite of the above possible misgivings about the fundamental applicability of eq 1, our rationale for including the rather lengthy discussion on this topic in the Supporting Information section is that we believe this discussion to be useful to those who are interested in describing the details of DBS gel structure and its aging processes. Indeed, we made an effort to consider different possible underlying processes during aging and how the data support or do not support these mechanisms. Also, we included other NMR measurements that might be of more general interest but bear on certain mechanisms of aging. (For example, proton transverse relaxation times were measured for the in situ gels, and on the basis of these measurements, it was qualitatively determined that there are two populations of DBS, those in the solid and those in solution. On timescales of tenths of seconds, chemical exchange is negligible between these groups. The corollary statement is that molecules in solution that come into contact with a DBS gel particle have residence times on the gel particle of less than 0.1 ms before desorbing again. This suggests that even though DBS in acetone has a modest solubility this does not mean that there is a rapid remodeling of the DBS fibrils via the fast exchange of DBS molecules between solid and solution.)

Conclusions

NMR is shown to be a powerful and versatile method for characterizing DBS gels both in situ and in dried forms. The DBS nanofibrils are seen to have order but not true crystalline order (i.e., ordered domains do not have a uniform unit cell throughout). These nanofibrils are made up of rigid molecules, are reinforced by strong hydrogen bonds, show modest additional mobility near the fibril surface, and are free of solvent in their interiors. The effort to identify a DBS crystalline structure related to the ordering of the nanofibrils was partially successful in that only one component of a mixed crystalline sample showed a structure related to the fibrils. However, because this mixed crystalline structure was derived by solid–solid transformation from a different crystal structure and because the two components of the mixed crystal

(45) Watase, M.; Nakatani, Y.; Itagaki, H. *J. Phys. Chem. B* **1999**, *103*, 2366.

showed mixing on a scale of no larger than 20 nm, it is possible that this component crystalline phase is also subject to issues of limited lateral growth, similar to what happens in the fibrils. In any case, it does not seem very promising to propose an X-ray characterization of the mixed crystalline phase at this point in order to learn about the gel structure, owing to the problem of separating the contributions from each phase. Thus, if prospects are poor for obtaining a good X-ray crystalline structure, identifiable with the gel structure, then it is significant that any proposed structure for the gel state, based, for example, on molecular modeling, satisfies the condition of strong H bonding for all pendant hydroxyls.

The buildup of stress in a twisting structure seems a plausible reason for the limited lateral growth of the DBS fibrils, but this has not been proven conclusively in this work. Of possible relevance is the fact that the DBS crystal structure formed at high temperatures from the melt by air cooling is characterized by (a) heterogeneous, weak hydrogen bonds and (b) the reversible ingress/egress of water whereas the contrasting gel structures, formed at much lower temperatures, are (a) impermeable to water and (b) possess strong hydrogen bonds. Given that hydrogen bonds compete with thermal energies much more effectively at lower temperatures, the implication is that an important driving force for molecular packing in the gel state of DBS is hydrogen bonding. The formation of such bonds in the nucleating stages of gel formation may be an important mechanism for bypassing the high-temperature, truly crystalline phase and dictating an

alternate template for fibril organization (along with its associated characteristic of limited lateral growth).

We have introduced a power-law equation that well describes the slow evolution of DBS concentration in acetone solution after the initial gelation has occurred. Of the mechanisms we have entertained to explain the slow evolution of DBS concentration in acetone solution in the presence of the gel, we favored (Supporting Information) the idea that the solid-state rearrangements necessary for pitch reduction in a helical structure are responsible for this effect. Further support for such a claim must certainly involve a rigorous investigation of the evolving gel morphology (e.g., using electron microscopy to observe a corresponding evolution in pitch or fibril width with aging). Longer-time measurements of c_{∞} at different concentrations would also aid in determining the validity of eq 1.

Acknowledgment. This article is an official contribution of the U.S. National Institute of Standards and Technology.

Supporting Information Available: Contents have been referred to variously in the above text. Notable are the NMR pulse sequences used and a discussion of the rationalization for eq 1 as well as more speculative comments regarding the mechanism that gives rise to DBS-concentration changes during gel aging. This material is available free of charge via the Internet at <http://pubs.acs.org>.